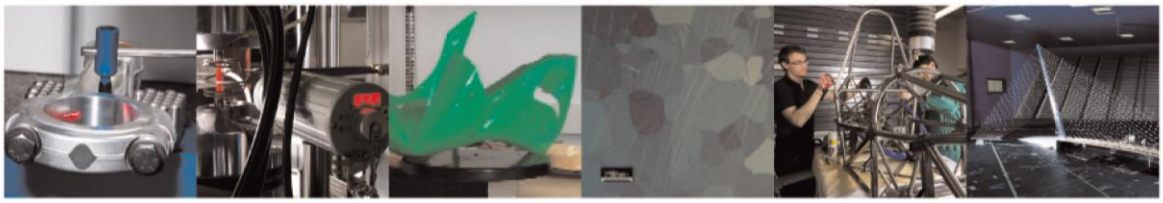

Surface footprint in molds micromilling and effect on part demoldability in micro injection molding

Parenti, Paolo; Masato, Davide; Sorgato, Marco; Lucchetta, Giovanni; Annoni, Massimiliano

This is a post-peer-review, pre-copyedit version of an article published in JOURNAL OF MANUFACTURING PROCESSES. The final authenticated version is available online at: http://dx.doi.org/10.1016/j.jmapro.2017.05.024

Surface footprint in molds micromilling and effect on part demoldability in micro injection molding

Parenti Paolo[1], Masato Davide[2], Sorgato Marco[2], Lucchetta Giovanni[2], Annoni Massimiliano[1]

[1] *Politecnico di Milano, Dept. of Mechanical Engineering, Via La Masa, 1 – 20156 Milan, Italy*

[2] *University of Padova, Dept. of Industrial Engineering, Via Venezia, 1 - 35131 Padova, Italy*

Corresponding author: email: paolo.parenti@polimi.it; Tel. +39 02 2399 8530; Fax + 39 02 2399 8585

Abstract

Accuracy of micromilled molds play an important role in complex process chains enabling mass production of polymer micro components, such as lab-on-chips, fabricated by micro injection molding. Surface footprint of micromilling is defined as the technological signature left by machining process on the generated mold surface. This is sensitive to selected tools and machining parameters and, when not controlled properly, can badly affect mold topography and functionality (e.g. part demoldability). In case of complex mold geometry, the impact of micromilling footprint increases, in particular during the demolding phase due to the friction generated by the polymer shrinking around cores. This work studies these effects on molds characterized by sub-millimetric cylindrical cores. A physical and statistical modeling was developed to provide deep insights about the effects of milling strategies and cutting parameters on the generated footprint on the mold cores. These effects are investigated by machining cylindrical pins whose roughness and surface form errors, caused by static deflection of tool and parts, were controlled in the range of S_a=150-400 μm and ΔR_{max}=1-10 μm (profile radial deviation), respectively. Micro injection molding experiments proved that mold topography has a relevant effect on the ejection force. The demolding force generated by a specifically developed polystyrene micro part reached the highest value with the mold machined with the most unfavorable milling conditions. Proper controlling of machine parameters and conditions led to a reduction greater than 60% of the demolding force peak, confirming the feasibility of the conjunct approach to processes optimization. The results of this work move a step forward into the integrated optimization of micro manufacturing process chains.

Keywords*:* Micromilling footprint, Surface texture, Micro injection molding, Demolding

Highlights

- Micromilling footprint is characterized for different cutting conditions
- Surface topography is characterized through interferometer microscopy
- An analytical model predicts the errors induced by tool-part deflections
- ANOVA investigates the cutting parameters/strategies effects on molds texture
- Micromilling footprint affect the ejection forces on molded parts

Graphical Abstract

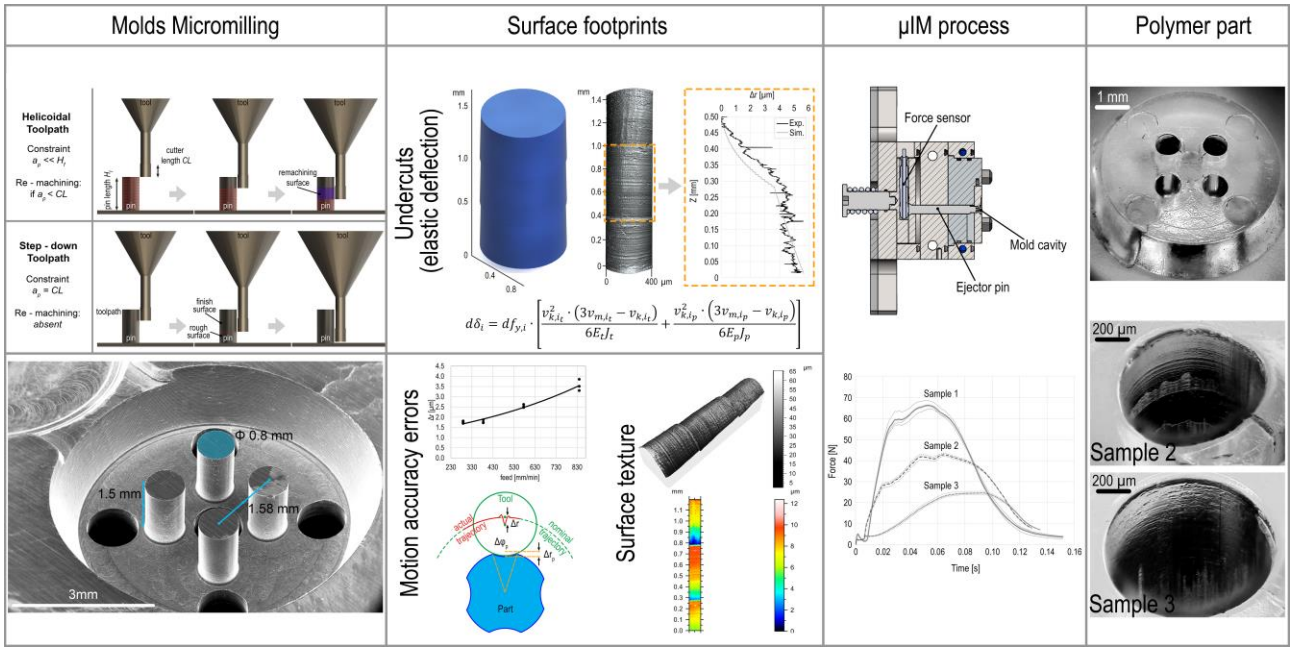

NOMENCLATURE (Symbols and Abbreviations)

a_e	Radial Depth of Cut	φ_j	Angular Position of each Flute j
a_{eff}	Radial Depth of Cut	φ_p	Cutter Pitch Angle
a_p	Axial Depth of Cut	φ_t	Cutting Engagement Angle
a_{p_max}	Maximum Axial Depth of Cut	h_n	Nominal Chip Thickness
A_D	Nominal Chip Area	H_f	Total Pin Heigth
β	Tool Helix Angle	$J_{t,p}$	Moment of Inertia
CL	Maximum Cutter Length	K_r	Radial Cutting Pressure
C_r	Corner Radius of the Tool	K_t	Tangential Cutting Pressure
ΔR_{max}	Maximum profile deviation of the pin	$L_{eng,t}$	Total Tool Shank Length
$d\delta$	Infinitesimal Deflection	$L_{p\text{-}Max}$	Active Length
df	Infinitesimal Force	µEDM	Micro Electrical Discharge Machining
D	Tool Diameter	µIM	Micro Injection Molding
D_{con}	Shank Diameter	µM	Micromilling
D_f	Finished Pin Diameter	n	Spindle Speed
$E_{t,p}$	Elastic Modulus	N	Tool Teeth Number
f_z	Feed per Tooth	r_{ce}	Cutting Edge Radius
F_r	Radial Cutting Force	S_a	Average Areal Surface Roughness
F_t	Tangential Cutting Force	v_c	Cutting Speed
F_x	Cutting Force in X-Direction	$v_{m,k}$	Force and Displacement Fixture Distance
F_y	Cutting Force in Y-Direction	V_f	Feed Speed
F_R	Resultant Cutting Force	z	Number of Tool Cutters
φ_{he}	Angular Delay of the Helix	z_i	Discretized axial contact point

Surface footprint in molds micromilling and effect on part demoldability in micro injection molding

1. Introduction

The relationship between surface texture and components functionality is getting more and more interesting in micro engineering applications. The case of molds produced by micromilling (μM) is interesting since the footprint generated on mold surface by μM plays an effect on the replication process and on the quality of the produced micro parts. In mass-production of polymer biochips produced by micro injection molding (μIM) the molds require complex features, such as multiple cores, to generate the interconnection holes through which a fluid moves inside the device. Good control of surface texture of the mold cores is mandatory to facilitate parts demoldability, allowing the production of functional and reliable biochips. To cope with this issue, two main requirements are mandatory: good geometrical/dimensional accuracy of the mold and a good mold surface finish. Masato et al. have demonstrated that the interlocking at the part-tool interface can negatively affect the μIM process when molds are affected by manufacturing errors such as burrs or geometrical deviations of the cores [1]. Increased mold roughness affects the appearance of the injected product but at the same time, affects the friction developed by the polymer parts when ejected from the mold. This increases the risk to induce deformations or cracks in the molded parts, thus invalidating the production process. Several studies at macro level claim that the higher the roughness the higher the required ejection force during the demolding phase, even if in some cases low roughness levels generate an increase of the force [2]. Moving to the micro scale, the increased surface to volume ratio worsens the effects of the interface boundary conditions making them crucial for the μIM process performance [3]. Micromilling is nowadays one of the most flexible and productive process to fabricate micro molds [4]. Compared to other micro manufacturing processes, such as micro electrical discharge machining (μEDM), μM gives higher productivity rates whilst maintaining similar geometrical accuracy, even on complex parts. Additionally, μM does not require part electrical conductivity and does not induce material substrate damages as μEDM does [5]. However, in respect to traditional milling, μM requires higher machine accuracy and finer parameter selections to cope with increased process complexity and constraints. At micro scale, additional phenomena affect the achievable performance in terms of geometrical/dimensional/surface accuracy and also productivity [6]. Large ploughing action of milling tools and minimum chip thickness are some μM serious issues that cause burr formation, increased tool wear and high wear sensitivity with respect to cutting parameters. In addition, the small dimensions and low rigidity of the cutting system, driven by micro tool compliance, is a source of location errors and shape deviations of machined components, which can lead in worst cases also to tool failure [7].

Cutting large aspect ratio pins in multiple configuration worsen these limitations due to the additional flexibility coming from the workpiece features and also from the limited tool diameters which are needed to machine close pins i.e. with small pin-to-pin center distances.

A good planning of μM involves the use of ultra-high precision milling machine and spindles, equipped with precise tool presetting systems [8]. On these machines, three-axis configuration is usually adopted for machining pins and other cylindrical features — as required by the molds for microfluidic devices — since it provides more reliable accuracy performance in respect to five-axis configuration [9],[10]. Micromilling accuracy is related with machine accuracy but also with process parameter selection as the authors have demonstrated in a previous work coping with the production of extremely high aspect ratio pins and with their dimensional and geometrical tolerances [4].

On the other side, the achievable surface roughness in μM is hard to predict in respect to standard macro milling process where indeed pure kinematic analysis of the cutting leads to good predictions [11]. Despite the aim to control footprint and texture generation in μM is a recent issue, nowadays, there is not a sufficiently wide amount of reliable information to solve real industrial cases.

Multiple models both theoretical-based and experimental-based exist in literature to predict surface topography. However, they lack of sufficient generality in particular in reproducing different tool shape and material behaviors. Moreover, despite they can predict kinematic component of surface generation to a good extent, they usually do not take into account the surface texture variability, which is lead in many real situations by other fundamental aspects, such as microstructure inhomogeneity of workpiece, elastic recovery of material, chip formation/evacuation troubles (e.g. chip adhesion and chip re-machining), process vibration [12]. Clear examples of theoretical approach are the dynamic model presented in [13] and [14] which links the generated texture — kinematic component solely — with cutting forces in milled molds, taking into account tool run-out and deflection. The authors of [15] investigated the effect of forces on burr formations and surface quality in titanium milling by setting a model that takes into account the main kinematic factors, including tool run-out and tool edge radius. In [16] authors proposed a model to simulate the surface generation process during μM of multiphase materials, considering the effects of cutting tool geometry, of feed rate and of part material microstructure. Other authors proposed a model aimed at optimizing μM parameters to increase texture functionality in case of nozzles machining [17]. Despite the reported relevant findings, results cannot be generalized to different surface geometries, different materials and different tool shapes, and therefore the ability to describe real complex cases with highly compliant features, as the studied one, is inhibited. In this regard, previous studies of the authors investigated the relationship between process parameters and achievable quality in case of thin wall manufacturing [18] and pin manufacturing [4] but texture generation was not investigated. Some enabling technologies are needed to cope with μM texture generation: 1) to measure texture with sufficient accuracy; 2) to use synthetic indicators that reflect tex-

ture functionality 3) to perform experimental tests that isolate the effect of cutting parameters on texture from all other process variability source. Nowadays, it is a common practice to perform functionality tests of the surfaces without proper measurement support. Being capable to obtain a texture measurement in 3-D micromilled features is certainly a complex task due to the small-involved dimensions and the reduced optical accessibility of some surfaces. However, up-to-date non-contact optical systems can be exploited to accomplish this task [19].

Most proper synthetic texture indicators must be defined basing on their capacity to describe surface functionality, but μM literature confirm that this aspect is not trivial. Authors of [20] analyzed tribological behavior of precise complex molds for metal forming collecting surface friction coefficients and linking them with areal parameters (S_a, S_q). It turned out that minimum a_e provides minimum friction but change from abrasion to adhesion friction makes minimum S_a not corresponding to minimum friction. In [21] an amplitude *S* parameters-based analysis is performed about the effect of tool inclination onto the surface integrity and cutting speed in a finishing milling operation. The study ends up with results about the significant correlation between Skewness and Kurtosis parameters and the increase of lead angle in milling. Despite all this facts, currently available literature provides the understanding of most relevant machining parameters capable to affect different textures in μM, namely depth of cut [14], feed per tooth [15], milling strategy and spindle speed [22],[23].

The complexity driven by workpiece geometry increases when high aspect ratios features, as the studied cylindrical pins, are considered and dedicated investigations are required to understand the texture generation in relation to reduced static stiffness of the parts, with the aim of better monitoring and controlling the cutting process.

Following these considerations, this work investigates the footprint generation in micromilled molds for μIM and it studies the effect that surface finishing of mold cores has on mold functionality, in terms of demolding forces during polymer parts ejection.

Henceforth, the paper is organized as follows. First, μM footprint is defined and modeled considering 1) surface location errors caused by system elastic deflection, 2) marks caused by motion error of the machine and 3) texture effect. Then, design and cutting of μM specimens and design and setup of μIM are described along with the adopted measurement procedures. Eventually, the paper discusses the conducted experimental campaigns aim at investigating the effects on the demolding forces.

2. Material and methods

Micro cylindrical cores, i.e. micro pins, with 0.8 mm diameter and height of 1.5 mm were considered as the geometrical features of interest. These features are used in biochips' molds for producing the interconnection holes inside the devices and their surface quality is fundamental for the determination of the ejection forces in μIM.

Since final topography of the mold cores depends on μM surface footprint generated during the finishing phase, different strategies were tested in this work, conducting both modeling and experimental based investigations.

2.1. μM finishing strategy

The pins specifications, namely the dimensional/geometrical accuracy and the surface finishing, require the adoption of specific μM strategies for finishing machining phase. Usually, flat-end or round-end micromills are adopted and industrial practice and tool manufacturers tell that the best roughness and geometrical quality are achieved with end mills in a three-axis configuration with a "top-down helicoidal" strategy around the pins. This strategy leaves larger stock on the part during pin cutting — i.e. during the rotations of the mill around the main pin axis — in the same way the step-support type does in thin-walls milling [18]. This limits the part deflection and the final geometric deviations on the part. However, this configuration is not always optimal since continuous overlapping and re-machining of the surface occur. In particular, this happen when, trying to maintain low force levels, the selected a_p, i.e. the pitch of the helicoidal strategy, is imposed as lower than the total axial cutter length. On one hand, this phenomenon helps generating shiny-look surfaces but on the other it has a main drawback that consists in larger contact time between tool and workpiece that causes increased wear and production costs.

Surface re-machining and dwelling makes texture generation difficult to predict and to control and therefore has to be avoided to reach repeatable machining behavior and to reduce tool wear. In this regard, use of a five-axis configuration with helicoidal toolpaths, with a tool axis misaligned in respect to pin axis, can avoid it. Unfortunately, in micromachining not all the cases are suitable for five-axis configuration, such as the narrow pin arrays where the reduced pin-to-pin center distance prevents the application of the required misalignments.

Indeed, re-machining can be avoided by adopting a three-axis "constant step-down" approach, which performs the finishing operation by cutting the pin plane-by-plane, with full axial engagement of the end mills. In this approach, the tool follows a circular path with constant axial position around the pin, then it realizes a step in vertical direction and then it repeats the circular paths until the pin bottom end is reached (Figure 1). The number of steps to perform depend on the total cutter length of the end-mill and the total pin height. By imposing the use of large axial engagements i.e. equal to the total tool cutter length, this approach can enhance productivity. This is because, given a total pin height H_f, the contact time T required by finishing operation strictly depends on the axial depth of cut a_p (Eq. 1).

$$T = \frac{H_f}{a_p} \frac{z \cdot n \cdot f_z}{\pi \cdot D_f} \tag{1}$$

However, upper and lower boundary constraints on the other parameters, such as the radial engagement a_e and on feed per tooth f_z, exist. On one side, these parameters must be kept small to limit cutting forces magnitudes and the relative tool-part deflection, in order to limit the subsequently surface location errors on the part. On the other side, adopting such small values modifies the cutting action, leading to increased tool ploughing with subsequent detrimental effect on surface generation.

When machining miniaturized molds, selection of milling strategy for the best surface texture must take into account also the motion inaccuracy errors of the machine. These errors are usually lead by friction in the moving components, such as leadscrews and guideways and introduce localized surface defects on the surface. In this regard, their generation is in strict relation with the re-machining given by the helicoidal toolpath and the large axial depth of cut of the step-down approach, as discussed later.

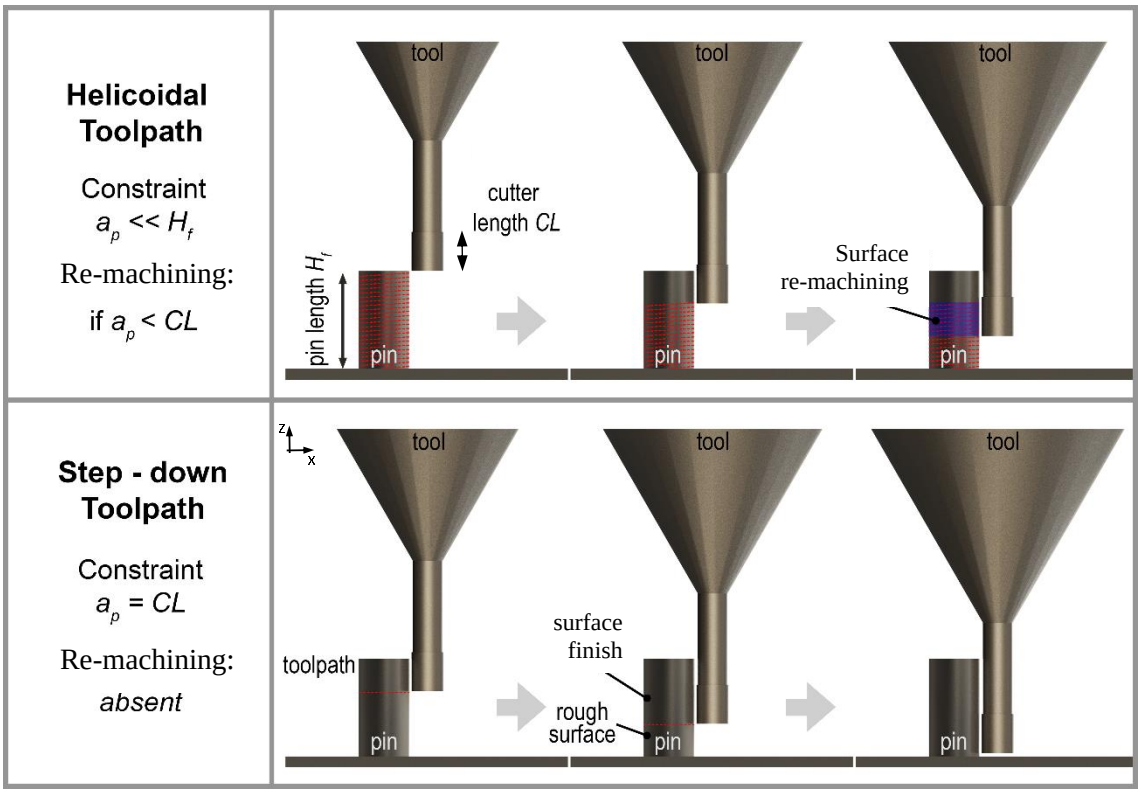

Figure 1: Pin finishing strategies (three-axis cycle)

2.2. Surface footprint modeling

In this study, the micromilling surface footprint on the cylindrical core features is defined by the following different contributes:

a) Localized surfaces marks caused by elastic deflection of tool and part (that act as undercuts in injection molding).

b) Localized surface marks caused by positioning accuracy of machine axes.

c) Distributed surface texture given by the conjunct effect of cutting kinematic (i.e. tool shape and trajectory), cutting dynamics (e.g. vibrations) and other random effects (causing for example smeared material, burrs and scratches).

The following paragraphs give detailed explanation of these effects. A mechanistic force modeling approach is adopted to describe the case *a*), whilst an empirical and statistical characterization model describes case *b)* and *c)*, respectively.

2.2.1. Surface errors due to system elastic deflection

The reduced static and dynamic stiffness during pin μM introduced by the tiny tool and workpiece shapes, represents serious concern for process accuracy. In fact, large relative deflection can rise up due to cutting forces, with consequent geometrical and surface errors on the workpiece. The generated cutting forces deflect the cutter away from the workpiece and extra amount of material is left on the finished surface. Both magnitude and direction of cutting forces are important for this aspect and a sensible moving direction, over which errors generate on the part, has to be identified from case to case geometry. This concern can be addressed by exploiting cutting process modeling to estimate cutting forces and consequent surface location errors produced by part and tool compliances, following the approach presented in [24] for a generic macro peripheral milling operation. In μM, additional force contributes rise, due to the relative reduced sharpness of cutting edges in respect to the nominal chip thickness and therefore macro cutting models need to be improved. Experimental evidence shows that this effect exacerbates the magnitude of tool deflection leading to surface deviations that can be comparable to cutter engagements, with related risk to reach part and tool breakage. Moreover, additional deflection contributes are given when machined features show low stiffness and this must be taken into account in modeling, since it leads to additional modification of tool-part relative trajectories. Structural dynamics may also play a role on surface location errors. Forced and self-induced vibrations may rise from the pulsing cutting forces and therefore a proper selection of cutting parameters is fundamental to prevent these occurrences [25] in relation to the specific system dynamic behaviour.

2.2.1.1. Cutting forces

A mechanistic force approach was developed in this work to estimate micro pins geometrical deviations and consequent undercuts on pins surface. The approach is contextualized for the studied case and acts as a support for cutting conditions setup, taking into account required part accuracy.

Tangential and radial cutting forces F_t and F_r can be modeled in μM, as proportional to removed chip area A_n [24] (Eq. 2):

$$\begin{Bmatrix} F_t \\ F_r \end{Bmatrix} = \begin{Bmatrix} K_t \\ K_r \end{Bmatrix}_{h_n, r_{ce}} \cdot A_n(\varphi_t) \tag{2}$$

Nominal chip area can be determined starting from nominal chip thickness h_n — which varies with engagement angle φ_t — and from axial depth of cut a_p — which is kept constant in the studied case — as $A_n(\varphi_t)=h_n(\varphi_t)\cdot a_p$. When tools have low radial run-out, when they adopt relatively low feed per tooth f_z and when the initial angular engagements of cutter into workpiece are neglected, nominal chip thickness can be approximated to $h_n= f_z \sin \varphi_t$. In presence of helical end-mills with multiple flutes — where cutter pitch angle is given by $\varphi_p =2\pi/N$ for a μM tool with N number of teeth — the engagement angle is a function of flute j, in particular $\varphi_{tj}= \varphi_t+j\varphi_p-\varphi_{he}$, with φ_{he} angular delay of helix (φ_{he}=tan β/D).

Computation of horizontal and vertical cutting forces, as measured in Cartesian reference frame X-Y plane, can be done as following (Eq. 3):

$$\begin{Bmatrix} F_x(t) \\ F_y(t) \end{Bmatrix} = \sum_{j=1}^{N} \begin{bmatrix} -\cos(\varphi_j) & -\sin(\varphi_j) \\ \sin(\varphi_j) & -\cos(\varphi_j) \end{bmatrix} \begin{Bmatrix} F_t \\ F_r \end{Bmatrix}_{h_n, r_{ce}} \tag{3}$$

Then, resultant cutting forces can be computed as $F_{R=}(F_x^2+F_y^2)^{0.5}$.

The specific cutting coefficients K_t and K_r for a micro cutting process are assumed a non-linear function of nominal chip thickness h_n, whose instantaneous value varies with engagement angle $\varphi_t(t)$. This particular assumption is done to take into account the cutting edge radius (r_{ce}) that typically develops strong effects as tool ploughing, in particular when instantaneous chip thickness is smaller than its value [26].

Basing on this consideration, cutting constants are defined as summation of two terms: one related to pure shearing action and a second describing the edge effect produced by cutting edge radius r_{ce} (Eq. 4)

$$\begin{aligned} K_t(h_n, r_{ce}) &= K_{t1} \cdot h_n(\varphi_t)^{-K_{t2}} + K_{t3} \cdot h_n(\varphi_t)^{-K_{t4}} \cdot r_{ce}{}^{K_{t5}} \\ K_f(h_n, r_{ce}) &= K_{f1} \cdot h_n(\varphi_t)^{-K_{f2}} + K_{f3} \cdot h_n(\varphi_t)^{-K_{f4}} \cdot r_{ce}{}^{K_{f5}} \end{aligned} \tag{4}$$

Each force component has five cutting coefficients that can be determined by dedicated cutting experiments involving acquisition of cutting forces and application of curve fitting methods. Experimental evidence shows that these em-

pirical constants mainly depend on coupling between workpiece material and tool geometry [27]. On the other side, they can be assumed invariant with respect to cutting speed and axial depth of cut, simplifying the analysis.

Once these parameters are determined, cutting forces can be estimated for a specific cutting configuration. When contouring curved geometries, as the studied pin case, chip area differs in respect to straight profiles cutting, due to different cutting engagement imposed by cutting kinematic. Effective radial depth of cut a_{eff} becomes lower than nominal radial depth of cut a_e, imposing a lower engagement angle φ_t. Eq. 5 and Eq. 6 describe this kinematic relationship:

$$a_{eff} = \frac{a_e\left(1+\frac{a_e}{2R_P}\right)}{1+\frac{R_T}{R_P}} \tag{5}$$

$$\varphi_t = a\cos\left(\frac{R_T - a_{eff}}{R_T}\right) \tag{6}$$

It must be noted that during external circular contouring, process kinematic imposes an actual machining feed at tool-workpiece contact point that is lower than the imposed feed to tool center point and therefore the f_z parameter, used for calculating forces, has to be re-computed in f_{zeff} (Eq. 7):

$$f_{zeff} = f_z \frac{\left(D_p + a_e\right)}{\left(D_p + D\right)} \tag{7}$$

2.2.1.2. Deflection computation

In the studied case, both deflection of the μM tool and of the part are considered. Only static deflection of the system elements was modeled and therefore the study is valid only for stable cutting conditions and it is not able to describe the additional problems rising from vibrated cuttings. The elastic compliance of these parts depends on their length, their cross-sectional shape, their material, the force application points and how the parts are supported. Micro-milling tool flexibility is modeled through a single fixed support cantilever beam, as done by [24], subjected to variable load amplitudes and variable load positions (Eq. 8). Moment of inertia is computed by considering a reduced equivalent diameter of the tool (D_{eq}=0.8*D), as suggested by [28],[24]. Static deflection of the pin is modeled similarly, by neglecting moment of inertia variability caused by material removal (according to the small finishing stock removal). Actual force contact point adopted in deflection computation is varied according to tool rotation and helical angle.

Due to the thin geometry of tool and workpiece, their relative displacement, caused by cutting forces, can be assumed as generated by static structural compliance solely — dynamic flexibility was neglected for simplicity. Workpiece fixturing and tool holder/spindle structures have much higher static stiffness and therefore they were neglected. The amount of deflection δ_i introduced in Y-direction by each elementary cutting force and generated on each axial discretization tool element *i*, can be computed as the sum of pin and workpiece displacements (Eq. 8):

$$d\delta_i = df_{y,i} \cdot \left[\frac{\upsilon_{k,i_t}{}^2 \cdot \left(3\upsilon_{m,i_t} - \upsilon_{k,i_t}\right)}{6E_t J_t} + \frac{\upsilon_{k,i_p}{}^2 \cdot \left(3\upsilon_{m,i_p} - \upsilon_{k,i_p}\right)}{6E_p J_p} \right]$$
$$\text{for } 0 < \upsilon_{k,i_{t/p}} \le \upsilon_{m,i_{t/p}}$$
$$d\delta_i = df_{y,i} \cdot \left[\frac{\upsilon_{m,i_t}{}^2 \cdot \left(3\upsilon_{k,i_t} - \upsilon_{m,i_t}\right)}{6E_t J_t} + \frac{\upsilon_{m,i_p}{}^2 \cdot \left(3\upsilon_{k,i_p} - \upsilon_{m,i_p}\right)}{6E_p J_p} \right] \quad (8)$$
$$\text{for } \upsilon_{k,i_{t/p}} > \upsilon_{m,i_{t/p}}$$

where υ_m represents the distance of the tool and pin fixtures from the point in which the force is applied and υ_k represents the distance of the tool and pin fixtures from the point in which the displacement is computed (Eq. 9):

$$\upsilon_{k,i_t} = L_{eng,t} - z_i;\ \upsilon_{m,i_t} = L_{eng,t} - z_i;$$
$$\upsilon_{k,i_p} = z_i;\ \upsilon_{m,i_p} = H_f - a_p + z_i; \quad (9)$$

It should be noted that the proposed modeling neglects torsional compliance effects, since they are orders of magnitude smaller than flexural effects in the studied case.

Total instantaneous deflection $d\delta_{tot,i}$ at axial contact point z_i is computed by superposition effect as the sum of all the $d\delta_i$, produced by the elementary force contributes, $df_{y,i}$.

2.2.1.3. Surface form error computation

Tool deflection generates a surface location error on part surface only when the cutter is in contact with the finished surface (i.e. φ_t=π/0, for a downmilling operation). Therefore, to estimate the surface location error along a circular coordinate of the pin, the relative tool/pin deflections at each finished surface angles φ_t produced by the tool during its trajectory has to be recorded. Actual tool trajectory allows to produce the final workpiece error map. In the step-down toolpath approach surface is generated by three cutting passes and therefore the angular position —developed by the tool around the pin during feed movement — equals the pin circular coordinate for a given Z-quote. Clearly, the three cutting passes performed at different Z coordinate values will correspond to three computed surfaces — affected by de-

flection errors in a different way — since static stiffness increases with Z. The deviation estimation approach can be adopted also in case of helicoidal strategy, where the tool moves along a spiral trajectory reaching the pin base. In this case, the developed force modeling can be assumed valid only at the beginning of the cut where the tool does not dwell on machined surface. The tool sections not engaged into cutting develop in fact additional frictional and plastic deformation force contributes that are not modeled and that can thus lead to an underestimation of the overall surface deviation error.

2.2.2. Surface errors due to machine motion accuracy

Micromilling surface footprint is also affected by motion accuracy of the machine. When conducting high-speed circular motions in the X-Y plane with small radii, as in the case of pin machining, tool center trajectory can deviate from the nominal one due to guideways friction and inertial loads. Linear motor and hydrostatic/aerostatic guideways can be used to develop machine tools with friction-less drive systems that are less prone to generate this kind of defects [29]. However, adoption of these advanced systems is not always possible and standard machine configurations with screw driven, ball guided positioning linear slides are usually adopted. To evaluate circular motion errors, load free motion tests can be executed prior to machining, adopting special grid encoders mounted on tool tips or simply reading the deviation from machine linear drives encoders and both these methods are suitable on small and rigid machines.

Since this error source is machine-and-trajectory dependent, no generalization is possible since coupled electromechanic system behavior —in relation to the system wear state — is hard to model with available modeling techniques. Therefore, empirical motion error characterization was conducted on the adopted μM machine.

2.3. Experimental setup

2.3.1. μM system

A state-of-the-art ultra-high precision milling centre (Kern Evo) with micrometric axes accuracy and repeatability was adopted. Proper clamping fixture was designed for the cylindrical ejector while the mold insert was placed using a standard fixturing system. A CAM software (CimatronE®) was used to produce the toolpath. Standard roughing and semi-finishing strategies were first conducted, then final pins surface were controlled by using the above-mentioned finishing milling strategies. Forces were acquired through a miniaturized top piezoelectric load cell (Kistler 9317B / 5015A) acquired at 51.2 KHz. The measures were compensated to reduce sensor inertial response through a model-based technique (details can be found in [4]). Additionally, in this latter case an AE sensor Kistler 8152B221 were installed on the machine fixturing for additional monitoring purposes.

2.3.1.1. Specimens design

Specific specimens were designed in this work to study footprint generation of µM process. The samples used for extended DOE analysis (Appendix) consisted in rectangular parts, obtained by starting from the same raw samples used for producing the molds tested in µIM (Figure 2). Each specimen contained 24 pins, with much more accessibility for post-process measurements in respect to the cores, with same geometry, designed on the molds (discussed later). Center-to-center distance of the pins was 2 mm in order to simplify µM roughing operations, using a 1 mm milling tool. In total, four different specimens were machined, by gluing/ungluing them on the fixturing system.

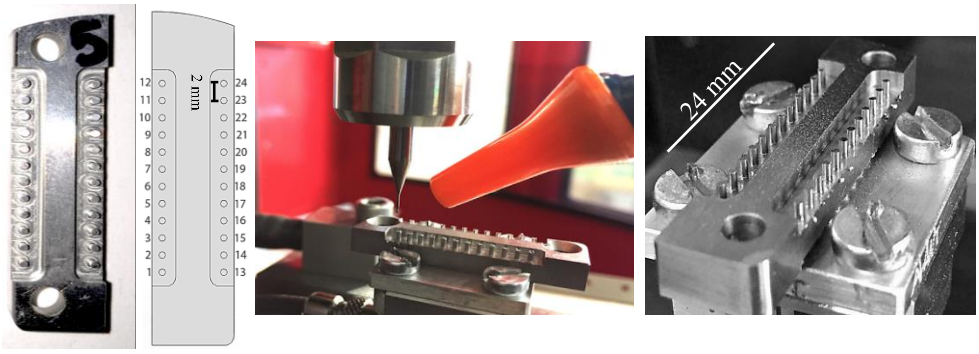

Figure 2: Setup of a specimen with 24 pins on the milling center

The specimens and the molds were made by a normalized stainless steel AISI420 (DIN 1.4021 - UNI X20Cr13, annealed), selected because of its wear resistance and toughness. The measured material hardness resulted in 18 HRC.

2.3.1.2. µM experiments (DOE)

The µM experiments on the specimens — i.e. with accessible pins — were organized in two different plans. First, plan A adopts a helicoidal interpolation tool trajectory, whilst plan B investigates a top-down finishing approach.

Plan A is defined by a fractional factorial plan 2^{5-1} with three replicates, for a total of 48 runs (Table 1). There are some blocks in this plan. First of all, due to the dimensions of the specimen samples it was not possible to realize all the runs on one sample, therefore two samples were used. Another block was imposed on roughing operation. In fact, a_e depends on the machining allowance leaved by the previous operation. Since pins are distributed on two rows, it was decided to use only one rough operation per row, which means set two blocks for each sample, for a total of four blocks.

Plan B is defined by a full factorial plan 2^4 with three replicates, for a total of 48 runs (Table 2). The experiments were completely randomized in spatial and temporal order. Half of the runs were realized on one sample and the others on another one, making one experimental block. In addition, the plans adopted a semi-finishing operation in order to

better control the allowance on the pins, so that experiments can be completely randomized without the need to introduce further blocks. In the Plan B, a_p was set constant (according to the strategy) and only a_e was varied.

Table 1: Helicoidal strategy experiments — Plan A

Parameter	**Low (-)**	**High (+)**
n [krpm]/ v_c [m/min]	24/ 37.7	32 / 50,2
f_z *[mm]*	0.006	0.012
$A_n = a_e * a_p$ *[mm]*	0.0125*0.015	0.025*0.050
Tool type	REM	FEM
Configuration	Upmilling	Downmilling
Trajectory Strategy	Helicoidal	

Table 2: Step-down strategy experiments — Plan B

Parameter	**Low (-)**	**High (+)**
n [krpm]/ v_c [m/min]	24/ 37,7	32/ 50,2
f_z *[mm]*	0.006	0.012
a_e *[mm]*	0.010	0.020
a_p *[mm] – Tool type*	0.5 - REM	0.7 - FEM
Configuration	Downmilling	
Trajectory Strategy	Step-down	

The main reason behind the choice of two different factorial plans relies on the fact that the step-down approach of plan B imposed the adoption of the maximum axial depth of cut allowable from the tools' geometry, thus creating a mutual link between a_p and tool type, which was not present in Plan A. On the other side, parameters' selection followed different criteria based on the requirements of finishing operations i.e. surface quality and dimensional error magnitudes. It is a common practice to use low feedrates and radial width of cuts to obtain the required accuracy. The hardest conditions were chosen accordingly to machine acceleration constraints i.e. the capacity to follow required nominal feed during circular trajectory. Preliminary test confirmed that the most challenging condition, as the test #49 (Appendix), could be reached by the machine axes with required V_f= 768 mm/min.

Mill type choice must take into account workpiece geometry. In presence of deep pin arrays, constraints exist on both maximum tool diameter and minimum tool length. On molds with flat surfaces, as the studied samples, μM is typically conducted with two mill categories, namely flat end mills (FEMs) and round end mills (REMs). In general, FEMs are used when a feature with sharp edges is needed while reduced tool wear sensitivity of REMs is required when cutter robustness and cutter resistance are mandatory — e.g. hard-to-machine materials. In the study, two 0.5 mm diameter coated end mills (Union Tool) were selected (Table 3). Air-Blow was used as suggested by tool supplier. Cutting configuration — downmilling and upmilling — is another decision variable. Downmilling is mostly suggested by tools producers because it reduces tool ploughing and tool wear. On the other hand, cutting mechanism of upmilling causes

an increase of tool temperature but it generates forces that are directed against feed direction and that can introduce a stiffening effect into the system. However, the faster wear makes upmilling strategy less advisable for micro cutting operations.

Modification of radial depth of cut a_e could also lead to different surface finish and to different part geometrical deviations. This is because a modification of the radial engagement during last finishing pass is developed by changing the diameter of the raw pins to cut — this is done by planning the semi-finishing passes in the CAM software. With different raw pins diameters, their total static stiffness would change by modifying part deflections during finishing thus introducing additional effects on the surface generation.

Table 3: Cutting tools specifications

Tool Type	***D***	***D*$_{con}$**	**z**	***L*$_{p\text{-}Max}$**	***a*$_{p\_max}$**	***C*$_r$**
FEM	0.5 mm	4 mm	2	2 mm	0.7 mm	0
REM					0.5 mm	0.05 mm

The other parameters, as rotational speed N, feed per tooth f_z and cutting speed v_c must be chosen considering chip load and other constraints, as for example forced and chatter vibrations. To avoid surface re-machining in the experimental Plan B, a_p represents a constraint related with the mill type since was set at maximum length of the cutting edge $a_{p,\max}$. The two plans were designed accordingly, taking into consideration the overall availability of four different specimens allowing a maximum number of tests equal to 96 (i.e. 24 pins on each sample).

2.3.1.3. Pin characterization

Direct measurements were performed on the specimens' samples solely, which showed optical accessibility at the microscope. However, a complete geometrical characterization of the pins was not necessary for the purpose of this study and therefore only surface texture and surface form error were evaluated in terms of µM footprint.

A confocal-interferometric 3D microscope (Bruker Countor Elite™ K) stitching acquisitions were adopted. The acquisitions captured central area of each pin — on the outer half sides of the pins, which were optically accessible — with a dimension of 200 µm width per 1.500 µm height, to minimize the errors caused by the high curvature and the consequent low incidence angle of light, in the border areas. Images were consolidated by using a data restore algorithm, to remove optical artifacts peaks and outliers. Evaluation of roughness indicators was performed by removing form and waviness — by applying on the 3D dataset proper fitting algorithms already implemented in the microscope analysis software. Surface indicators were calculated considering a Gaussian Regression Filter with cutoff wavelength

of 80 μm (according to ISO 4287 [30]). However, cutoff wavelength did show low sensitivity on the pin surface comparison.

Due to the complex nature of μM process and its intrinsic variability, areal measurements were preferred to profile measurements to characterize the surface roughness, trough specific areal roughness parameters [19] and [31].

Roughness generation in μM is not purely kinematic because phenomena as ploughing and elastic recovery play a key role inhibiting the generation of typical directional surface marks. Moreover, when machining a complex feature — such as a thin pin — milling tool shape leads to additional interaction phenomena between tool and machined surface that may alter the finishing quality in a complex and random way. Height parameters are by far the most widespread parameters used to quantify vertical deviations of machined surface. In this work, S_a — i.e. the arithmetical mean height — was adopted to quantify the pin texture. Three different patches were used to compute three S_a values for each pin, in order to verify the regularity of generated texture along the entire pin length.

Measurement procedure can be summarized as: a) data restoring to remove outliers/artifacts, b) terms removal to pass from 3D to 2D removing pin form and tilting, c) data masking to provide a fine selection of just the most homogeneous and reliable data, d) Gaussian regression filter with cut off wavelength 80 μm high pass filter, in order to focus on roughness, e) S parameters computation to provide numerical value indicators.

Main variability sources affected the computed data as the pure variability of the cutting process, the variability induced by varying cutting parameters, the pure variability of the measuring procedure + post-processing on data clouds.

2.3.2. μIM system

A state-of-the-art μIM machine (Wittmann-Battenfeld, MicroPower 15) with a maximum clamping force of 150 kN and maximum injection speed of 750 mm/s was used for the experiments. The online monitoring of the demolding force was carried out using a Kitsler 9223A piezoelectric force sensor — connected to a Kistler 5039A charge amplifier and a National Instrument NI9205 acquisition board working at an acquisition rate of 60 kHz. The sensor was mounted behind a 6 mm ejector rod, as showed in Figure 4.

A commercial amorphous polystyrene (PS, Total PS Crystal 1540) was selected as the molding polymer for its high bio-compatibility that make it widely used for bio-components applications. Material density is 1.04 g/cm3 (ISO 1183), melt flow index MFI is of 12 g/10min (200 °C/5kg, ISO 1133) and glass-transition temperature Tg is of 100 °C (ISO 6721).

2.3.2.1. Mold insert design

The effects of the mold texture generated by the µM process were investigated in the µIM process using a specifically designed micro mold characterized by four deep cores (Figure 3). The presence of the four pins in the cavity allowed to maximize the total wetted area, significantly affecting the frictional forces generated during the ejection phase. Moreover, in order to isolate the contribution of the texture to the tribological conditions at the part-tool interface — i.e. to study how core surface finish affects the ejection forces — the outer surface of the mold cavity was tapered by 18 degrees. The pattern distance between the pins was designed based on the availability of commercial µM tools. Symmetric disposition of ejection holes around the mold center was designed to balance the ejection forces.

The demolding of the micro parts was realized by machining five cylindrical pins (1 mm diameter and aspect ratio of 3) on the top of a 6 mm ejector rod. The ejector material used was a hardened Tool Steel AISI O2 (UNI 90MnVCr8 DIN) with an average hardness of 50 HRC.

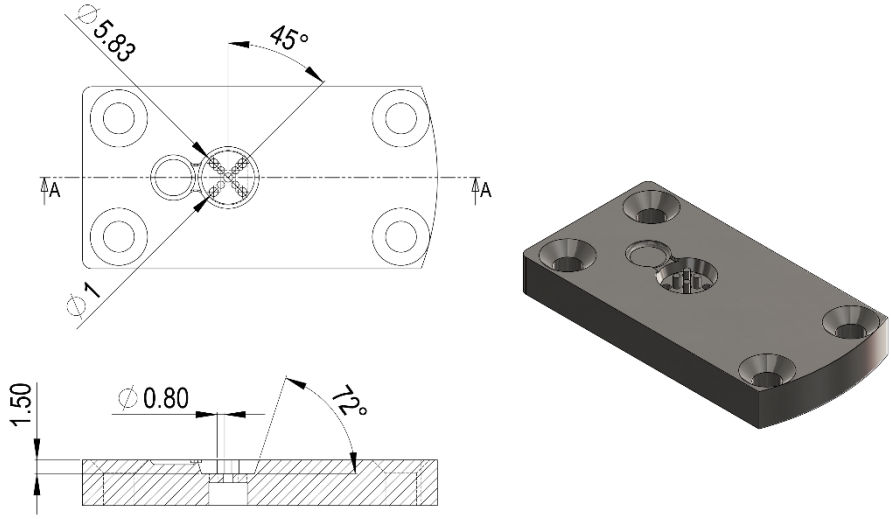

Figure 3: Designed mold insert with micro pins (SEM 50x)

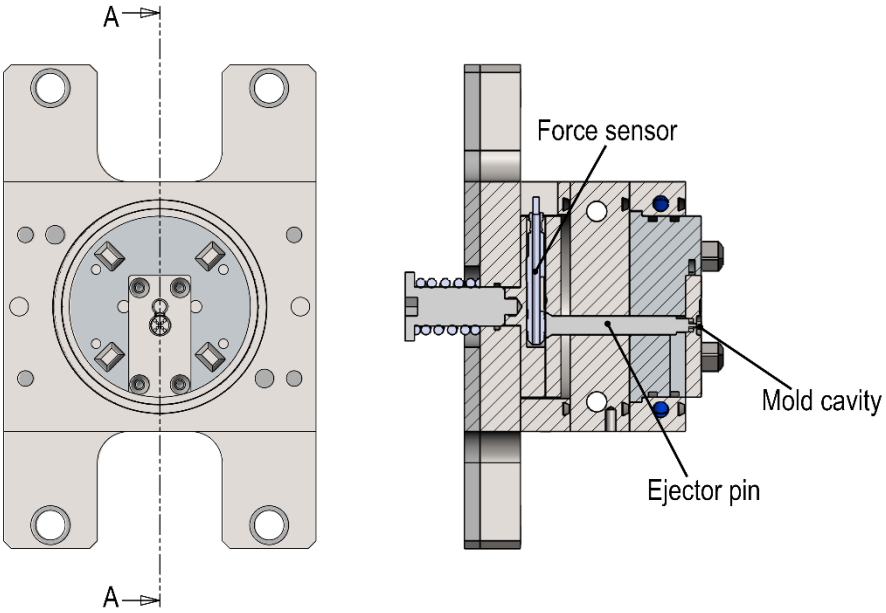

Figure 4: Mold assembly: a) real machine and b) force sensor scheme

3. Results and Discussion

3.1. Forces and deflection modelling

The force and deflection model was implemented in Matlab®, which was used also for model validation, i.e. post-processing experimental data. Cutting coefficients used to produce the numerical computations (Table 4) were taken from [25] that studied an AISI 1045 steel, with similar hardness and strength values in respect to the AISI 420 adopted in this study.

Given the irrelevant effect of tool run-out on part form error — in respect to the large contributes given by elastic deformation —and given the extremely low measured run-out of the adopted tools and machine spindle, this aspect has been neglected in the analysis, but it can be introduced in the modeling framework in a straightforward way, as done in [27]. Following values were set in the simulations: r_{ce}=4 μm E_t=600 GPa, E_p=210 GPa.

Table 4: μM Cutting coefficients

Cutting coefficients	**Tangential direction**	**Radial direction**
$K_{t1,r1}$	2447	1796
$K_{t2,r2}$	0.0108	0.0094
$K_{t3,r3}$	4305	2723
$K_{t4,r4}$	0.8176	0.8557
$K_{t5,r5}$	1.050	1.088

Good agreement was found between the acquired forces — after the application of the inertial filter discussed above to remove the first dynamometer resonance at around 3500 Hz — in mostly all the cutting conditions. Experimental cutting forces (Figure 5) stayed below 5 N of peak-to-peak resultant cutting force. No relevant tool run-out was revealed by force profiles. Some residues of the inertial disturbance response, excited by the high order cutting harmonics, were still visible in the force profiles — especially during the no-load cycle period that extends for about 1 ms every tool rotation. However, due to the high rigidity of the sensor, these residues were not introducing relevant dynamic disturbances into the system and on surface footprint generation. Despite that, experimental cutting forces show in respect to simulated ones very similar shape, magnitude and phase, confirming the validity of the hypothesis assumed by adopting the cutting coefficients in Table 4.

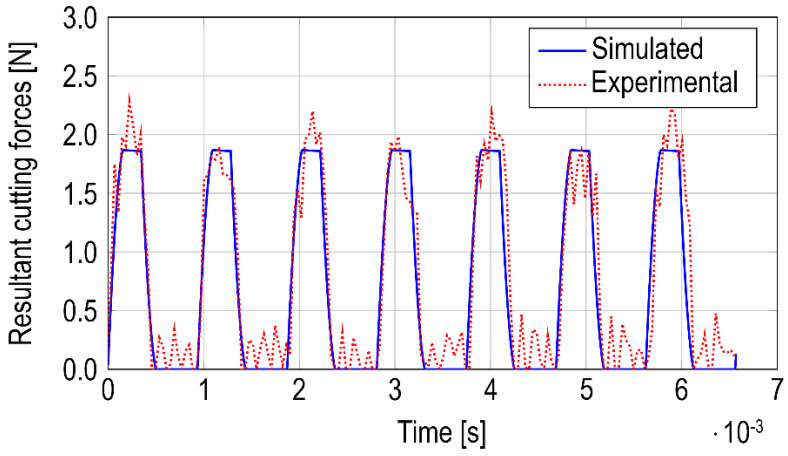

Figure 5: Simulated vs experimental cutting forces on test #91 (Appendix)

In addition, AE sensor and Force sensor analysis confirmed that stable cutting were reached avoiding any additional (and unwanted) vibrational contributes.

In the experiments, pin form errors, in terms of maximum radial deviation ΔR_{max}, ranged between 1 and 10 µm. Pins executed with step-down approach showed the expected undercuts, produced by the elastic deflection and tool trajectory. The modeling resulted capable to predict with sufficient accuracy also the profile deviations and the undercuts surface errors, which anyway dominated the profiles in respect to the underlining surface roughness.

The profile deviation of the cylindrical pins machined in Plan B shows three definite sections where the profile diverges in similar ways. By analyzing one of these sections, corresponding to one of the axial tool engagement steps, it can be noticed that almost half section length, Figure 6c, assumes an exponential profile deviation while the remaining half section deviates with almost a linear law. This fact — due to the conjunct effect on the tool angular engagement of tool helix angle and adopted axial depth of cut — is well predicted by the model, which estimates well the maximum

profile deviations $\Delta R_{max,i}$ that cause the surface undercuts for each of the *i*-section and that reach the maximum values at the top section. Similar agreement was found for the test executed in Plan A.

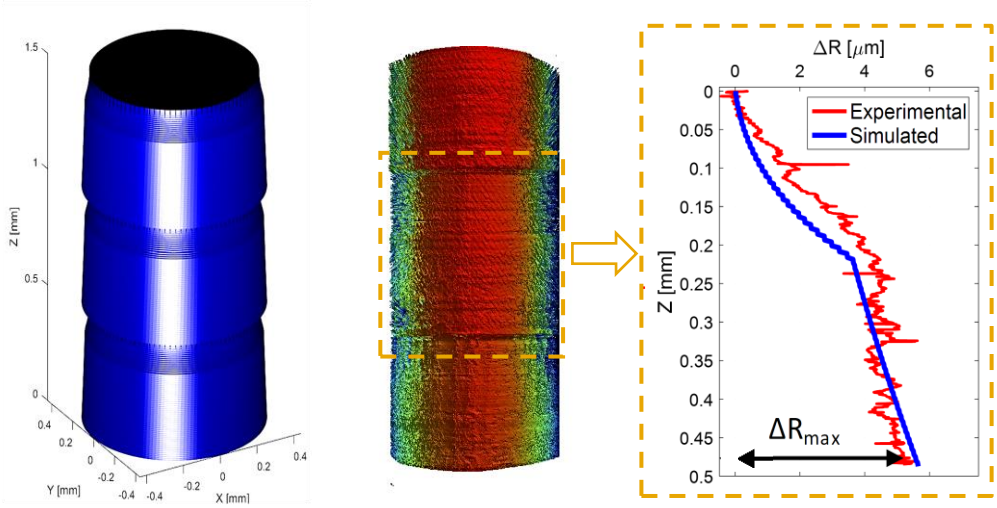

Figure 6: Surface Form error, test #91 (Appendix): a) simulated shape — error amplification 5x; b) WLI interferometer measurement; c) comparison experimental/simulated profiles — middle pin section.

3.2. Machine motion accuracy errors

In order to assess the motion errors and characterize empirically the system behavior and its effect on pin surface footprint, the nominal and actual axes displacements were acquired during the cutting. Figure 7 depicts the actual axes trajectory read by the linear axes encoder during surface pin finishing operations, for the three feedrates adopted in the DOE plan (Appendix). The adopted machine did not implement any advanced friction compensation scheme. Acceleration and jerk values on the axes drive were set to 8 m/s^2 and 200 m/s^3, respectively.

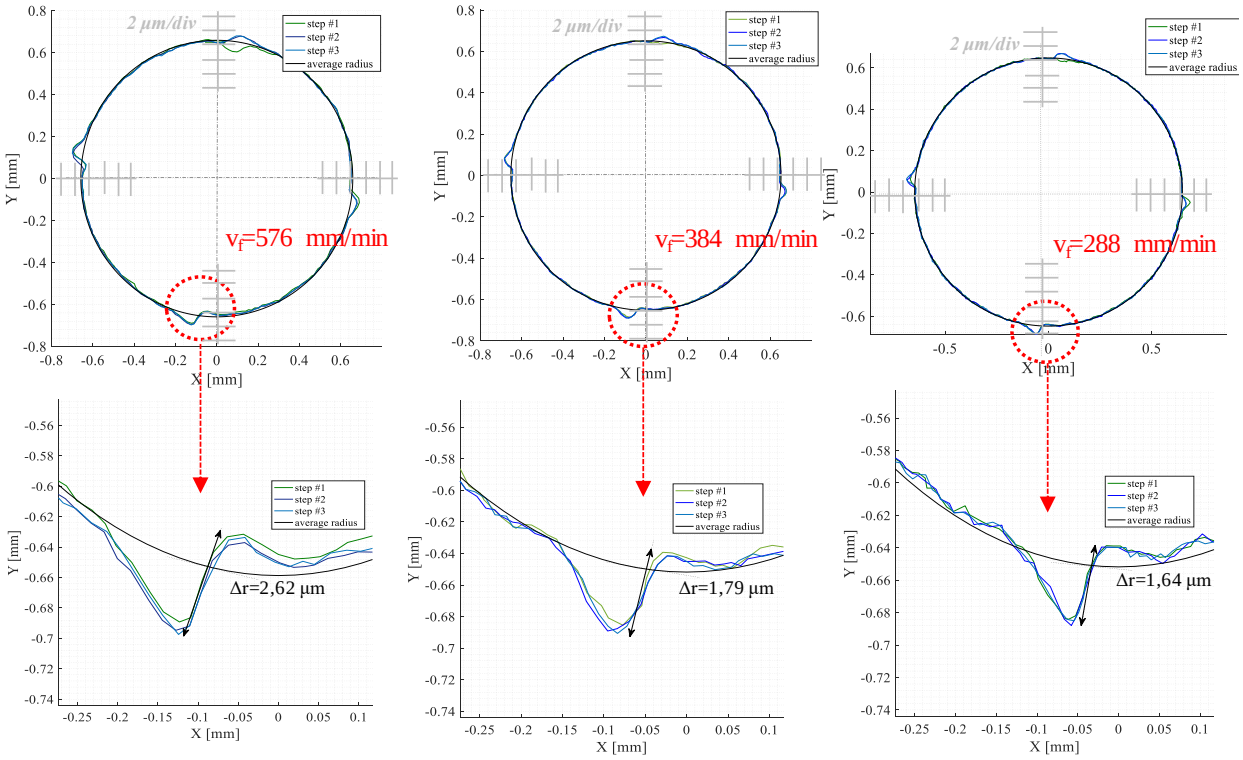

Figure 7: Motion error traces measured on adopted machine — error amplification 30x

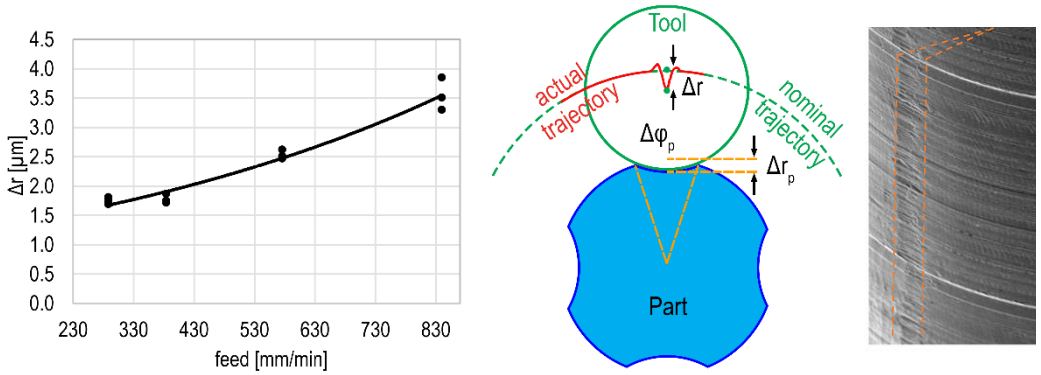

Figure 8: Relationship between feedrate and maximum deviation of tool trajectory.

For defining the surface footprint the localized geometrical defects caused by motion error were taken into account. In particular, four main zones related to X-Y axes inversion points were subjected to the most relevant motion deviations, as it typically happens. To quantify the surface local error, peak-to-valley tool trajectory deviation *Δr*, defined as normal to nominal profile, was used (Figure 8). In the tests, *Δr* demonstrated to be linearly correlated with the feedrate,

in the range 250-1000 mm/min, but always assuming sub-micrometric amplitude (from 1.6 to 3.9 μm). The milling tool transfers these deviations into surface texture marks, by smoothing the error profile thanks to its diameter, as it can be noticed in the produced parts (Figure 8).

Then, within the range of tested feed values, depth and angular extension of the defects— i.e surface location errors Δr_p and $\Delta\varphi_p$, respectively — can be approximated with the following relations (Eq. 10, Eq. 11)

$$\Delta r_p \approx \Delta r = 2.7e\text{-}6 \cdot v_f^{\,2} + 3.8e\text{-}4 \cdot v_f + 1.4 \tag{10}$$

$$\Delta\varphi_p = 2 \cdot \arccos\left(\frac{D_p/2 - \Delta r}{D_p/2}\right) \tag{11}$$

Despite these marks are clearly evident on the surface (Figure 8), their resulted vertical orientation — aligned with the demolding direction — together with their small angular extension, reduce their expected impact on mold functionality i.e. on part demoldability and ejection forces. However, the empirical characterization method proposed here, still represents a valid approach to obtain an estimation of these errors. These estimations can also be used to support the feed selection. In fact, the effects of the low μM cutting forces on motion error can be considered negligible making possible the a-priori execution of the characterization tests in no-load conditions, before cutting the parts.

3.3. Surface texture on the cores

Pin external surfaces were analyzed at the microscope. First, the generated texture appeared constant along the circumference of the pins, thus confirming suitability of the measurement method, based only on the external half side of the pins (optically accessible). No relevant wear on tool cutting edges were observed after machining one component. Therefore, this parameter was not considered as a major play role in the surface generation (Figure 9). Since in the industrial practice only sharp tools are usually adopted for the last finishing passes of micro molds the effect of the tool wear had not been investigated further in this work.

As expected, in both the experimental plans the block factor did not play a relevant role since the material of the two specimens were obtained from the same original workpieces.

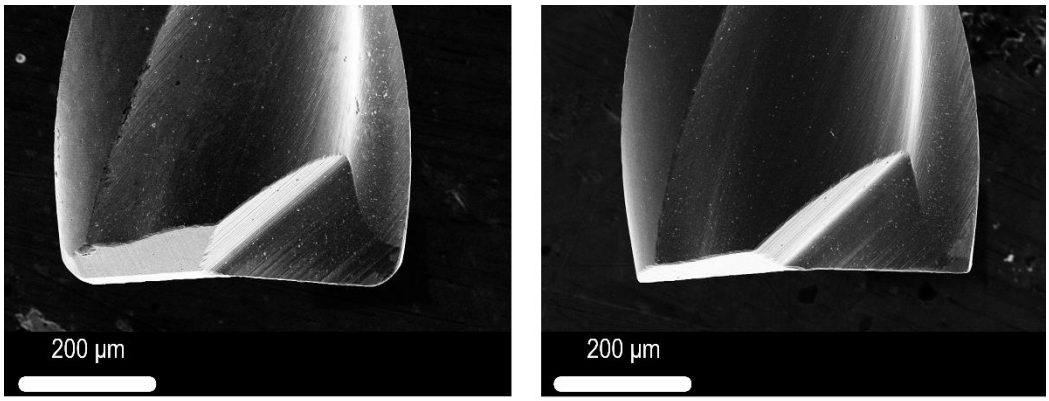

Figure 9: Micro end mills (SEM 500x). a) REM tool after machining 24 pins, b) FEM after machining 24 pins.

Results of Plan A — aimed at testing the helicoidal finishing— showed a general higher variability of surface roughness S_a among the three replicas. The generated surface textures varied a lot, ranging from surfaces with mostly smooth appearance but characterized by the presence of deep surface voids, to highly corrugated surfaces with smeared material that gave irregular topographies (Figure 10, Test #44 and Test #27). Surface with ploughing marks, scratches and other surface irregularities made the obtained pins, far from being characterized by regular and homogeneous surfaces. Typical periodic cutting marks that typically make the machined surfaces highly isotropic — i.e. whose features are independent from the direction along which they are analyzed — were absent in mostly all of the machined pins with the helicoidal strategy. From a quantitative point of view (Table 5), S_a ranged between 160 nm and 470 nm.

There was a big difference between the flat end mills (FEM) and the rounded end mills (REM), with the latter that ensured lower S_a values (in average almost -50 nm). At the 95% of statistical significance f_z resulted not significant but in a borderline situation (p-value 5.2%, Table 5) where its increase had bad effect on S_a. A couple of interactions did also play a statistically significant role, namely the tool type with the radial immersion a_e and the a_e with the cutting strategy. In particular, increasing a_e did increase the roughness on the REM tool whilst playing an opposite effect on the FEM tool. The same antithetic behavior was played by the strategy since downmilling provided better surfaces with the highest a_e value, whilst upmilling did better with lowest a_e values.

Table 5: ANOVA p-values for helicoidal strategy experiments — Plan A

Factor	**p-value**
Main factor	
tool	0.001
a_e	0.868
n	0.336

f_z	0.052
Strategy	0.0762
First order interaction	
tool · a_e	0.001
tool · f_z	0.182
a_e · n	0.899
a_e · f_z	0.416
a_e · *strategy*	0.002
n · f_z	0.174
f_z · *strategy*	0.878

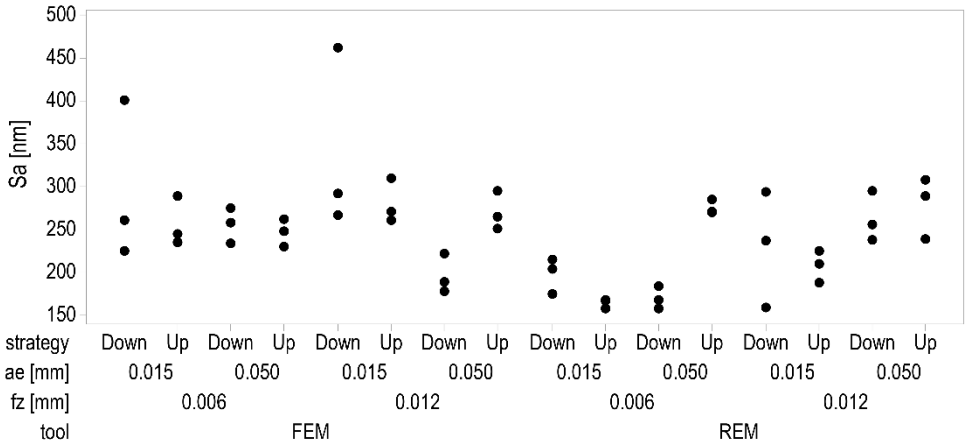

The plan B, carried out to test the step-down cutting approach, produced different results. First of all, most of the produced surfaces showed a regular texture, associated with feed marks, inclined by the tool helix angle i.e. 30°, (Figure 10, Test #95). In some of the pins, these kinematic marks were plastically deformed most likely due to the ploughing action of the tool increased by the elastic deflection of the tool and part, as discussed in the above paragraphs (Figure 10, Test #73). In general, this cutting strategy makes cutting parameters definitively more important and an overall reduced variability of the texture appearance among the replicas was found. In particular, the conducted ANOVA analysis confirmed that the tool type, the radial immersion and the feed per tooth were the main significant factor on the S_a (see p-values in Table 6). The REM tools guaranteed lower S_a values in respect to FEM tools, whilst bigger values of a_e and f_z conducted to an increase of roughness of almost +25 nm. In the tests, the achieved S_a ranged between 175 nm and 340 nm. Another noteworthy fact is that spindle speed was not a relevant factor for the average roughness determination. However, tool type showed some interaction with it and with the feed per tooth values. On one side, an increase of the spindle speed improved S_a when REM tools were adopted, but did the opposite with FEM tools. On the other side, REM tool appeared more sensitive to the selection of the feed per tooth, whose lower values led to the best results in terms of S_a, in respect to FEM tools which were not so affected by the feed per tooth selection.

This analysis confirmed that the micromilled surface topography has a significant impact on the pins by adopting different finishing strategies and cutting parameters. A better control of the topography was generated by adopting the

constant step-down approach, whilst the helicoidal strategy provided more irregular surfaces but with lower average roughness and characterized by less repetitive behavior.

Table 6: ANOVA p-values for step-down strategy experiments — Plan B

Factor	**p-value**
Main factor	
tool	0.000
a_e	0.000
n	0.937
f_z	0.001
First order interaction	
tool · a_e	0.619
tool · n	0.001
tool · f_z	0.018
$a_e \cdot n$	0.059
$a_e \cdot f_z$	0.589
$n \cdot f_z$	0.274

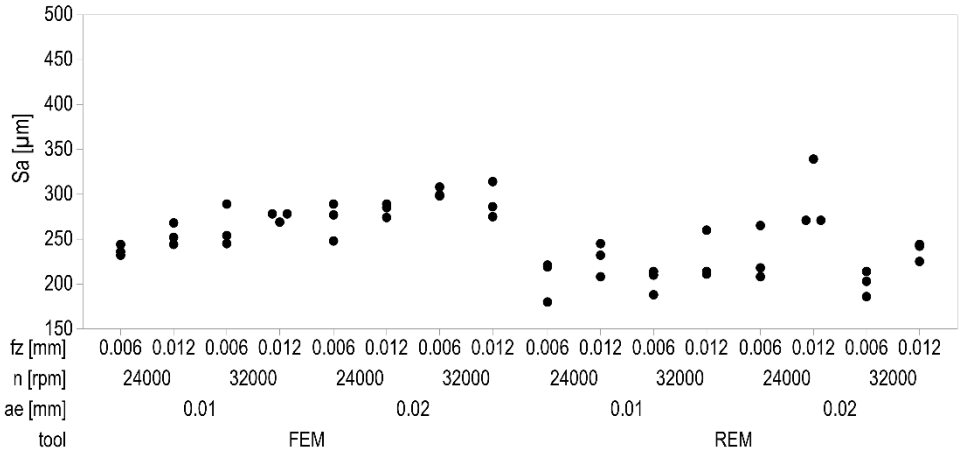

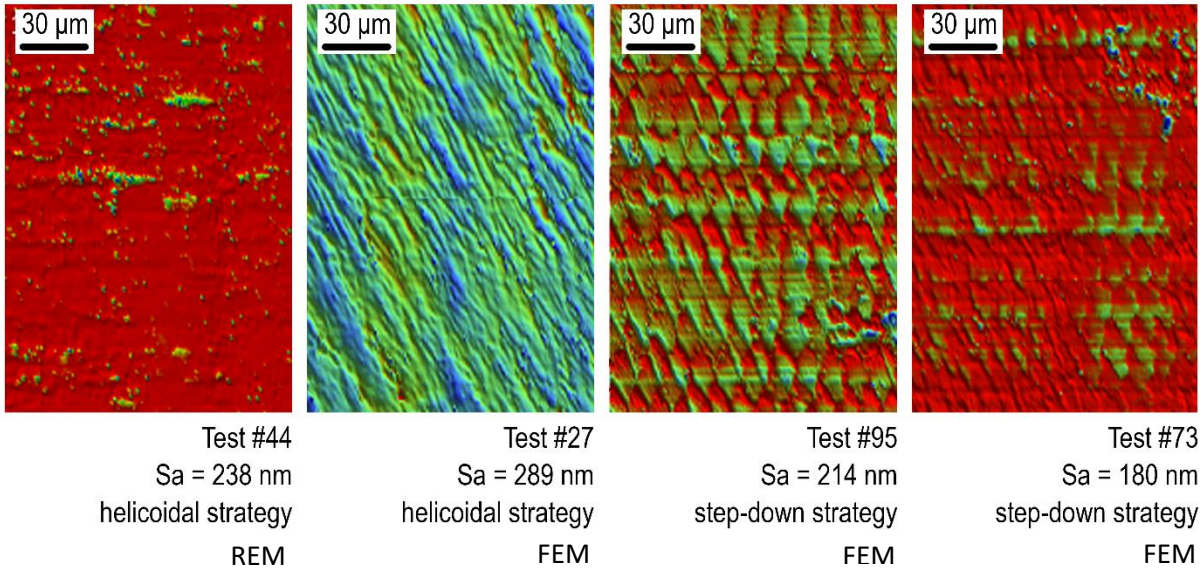

Figure 10: Measured roughness surface footprint

3.4. µM footprint effects on µIM process

The µIM tests performed using the three mold inserts machined with different µM strategies and parameters aimed at proving out the effect of the generated footprint on the demolding force reduction.

3.4.1. Mold machining and mold characterization

The parameters for the machining of the µIM mold inserts (Table 7) were selected according to the results of the DOE plan, as well as on the analytical modeling considerations regarding the surface location errors.

REM tools were used for machining the mold inserts, because of the low surface roughness obtained with them and also because in mold and die industry they are preferred for their lower corner wear sensitivity. The first two inserts (Sample #1, Sample #2) were machined with a step-down approach to generate the discussed undercut surface errors and test how they affect the demolding force. In order to generate surface defects with different amplitude, machining of Sample #1 adopted the harshest µM conditions characterized by a nominal uncut chip area that is twice that of Sample #2 (Table 7). Conversely, Sample #3 adopted the helicoidal strategy that was demonstrated to provide a smoother surface — but more scratched and smeared — without the presence of circumferential undercuts (Figure 11). Sample #3 adopted cutting parameters and down milling configuration in order to minimize the Sa value (Table 8).

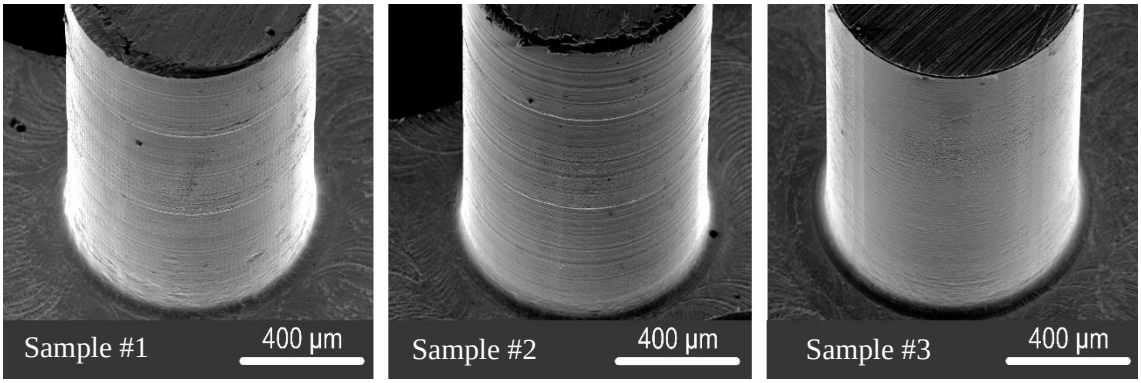

Figure 11: Machined molds for µIM experiments (SEM 400x).

Table 7: µM conditions adopted for machining the molds

Parameter	**Sample #1**	**Sample #2**	**Sample #3**
S [krpm]	24	32	24
a_p *[mm]*	0.5	0.5	0.0125
a_e *[mm]*	0.020	0.010	0.015
f_z *[µm]*	12.5	6	6
Strategy	step-down (downmilling)	step-down (downmilling)	helicoidal (downmilling)
Tool Type	REM	REM	REM

A preliminary SEM characterization of the machined inserts showed that they were characterized by different µM footprints, as can be seen in Figure 11. Each one of the generated mold surfaces is characterized by a homogeneous topography along its length — i.e. regularity along both the axial and circumferential directions.

According to their complex geometry restricting the optical accessibility, the characterization of the micromilled molds was performed by means of destructive testing (i.e. cutting of the mold inserts) after the µIM experiments (Table 8).

Table 8: Surface characteristics of the three micromilled molds.

Surface characteristic	**Parameter**	**Sample #1**	**Sample #2**	**Sample #3**
Undercut steps (elastic deflection)	ΔR_{max} *[µm]*	6.7	3.4	Absent
Inversion marks (motion error)	ΔR_p *[µm]*	2.7	1.9	0.9
	$\Delta\varphi_p$ *[rad]*	0.123	0.132	0.097
Average Areal Roughness	*Sa [nm]*	355	230	186

3.4.2. Ejection forces developed in µIM

Before the µIM tests were carried out, several dry cycles of the clamping unit were performed with a forward ejector stroke of 0.8 mm and a speed of 10 mm/s, in order to stabilize the coupling between the ejector pins and the correspond-

ing holes in the mold inserts. The dry force acquired for each mold insert was observed to be smaller than 1 N after 200 dry strokes, confirming the achievement of an adequate stabilization and functionality of the demolding system.

In order to directly compare the effects of different surface finish on the demolding force, the μIM experiments were performed adopting a fixed selection of molding parameters. In particular, the main μIM process parameters were set as follows considering the literature [32], recommendations of the material supplier and technological limits of the available experimental setup:

- mold temperature: 50 °C;
- melt temperature: 240 °C;
- injection speed: 100 mm/s;
- metering size 1.2 mm;
- packing pressure: 80 bar for 2 s;
- cooling time: 5 s.

In order to reduce the variability in the demolding force measurements, ten initial molding cycles were carried out to stabilize the process, then three force acquisitions were registered, one every five molding cycles.

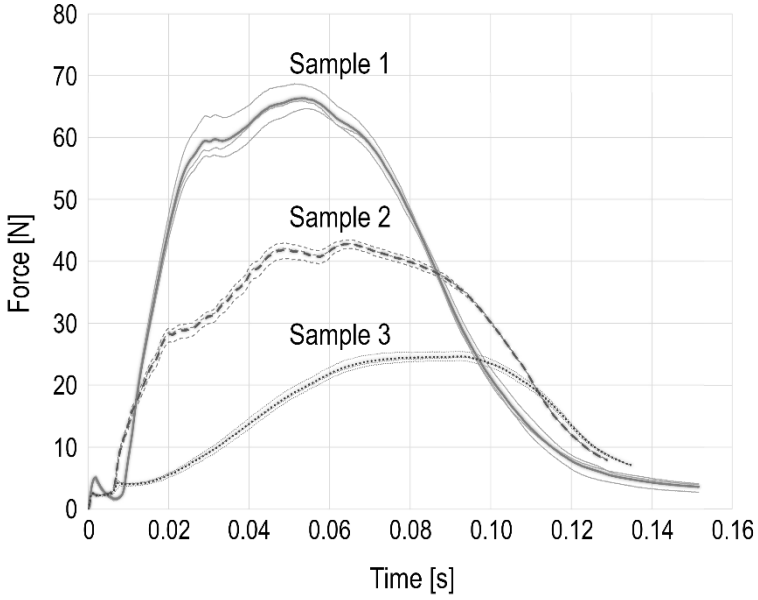

Figure 12: Acquired demolding forces in μIM tests

Figure 12 shows the demolding force acquisitions for each replication and each one of the three mold inserts. The average force (whoses profile is visible in Figure 12 as dotted lines) had similar trends, showing an initial steep increase, followed by a steady zone where the force peak was reached. After that, the ejection force had a soft drop until

the end of the ejection phase where it reached null values due to the complete separation of the part from the tool. The profile of the demolding force acquired with Sample #3 showed a smoother trend than those observed for Sample #1 and Sample #2, which showed more instabilities due to the more complex tribological interface interaction during the ejection stroke — i.e. increased part-tool interface interlocking caused by the circumferential undercuts related to the shape error.

The peak values of the demolding force acquisitions were considered as representative indicator for the analysis. Indeed, it is a critical parameter for the final quality of the molded part, being the maximum stress applied to the polymer part. In fact, the yield strength of the material must not be exceeded during the ejection phase in order to preserve the structural integrity and dimensional accuracy of the part, thus guaranteeing its final functionality.

The variance of the maximum force peak among the replicated acquisition was observed to be considerably smaller than the differences induced by the diverse mold surface finish. Specifically, the Coefficient of Variation (CV) was of 3.09% for Sample#1, of 1.58% for Sample#2 and of 3.04% for Sample#3, allowing the observation of the ejection force differences due to the different μM footprints.

The maximum demolding force was observed for Sample #1 whose pins are characterized by the highest surface roughness and the more marked shape error (Fe_{max}=66.45 N). The ejection force peak reduced by 35.5% in Sample #2 (Fe_{max}=42.86 N), which was characterized by reduced roughness and shape errors. The demolding stresses were minimized with Sample #3 (Fe_{max}=24.69 N), for which a reduction by 62.8% was observed, as a consequence of the negligible shape error and reduced surface roughness.

The results of the μIM experiments showed the high influence that mold topography generated by the μM process has on the demolding force. In fact, better surface finish favors the separation of micro parts from the tool, due to the less relevant interface adhesion occurring for improved μM surface footprint.

The mechanism behind the increase of the ejection force, due to the higher roughness is related to the interlocking that is generated at the part-tool interface during the filling and packing phases of the μIM process. Indeed, the pressure generated in the cavity leads to the replication of mold topography thus generating interface adhesion (Figure 13). Consequently, the ejection phase is negatively affected by a higher interface adhesion, which increases the force required to overcome the initial stiction.

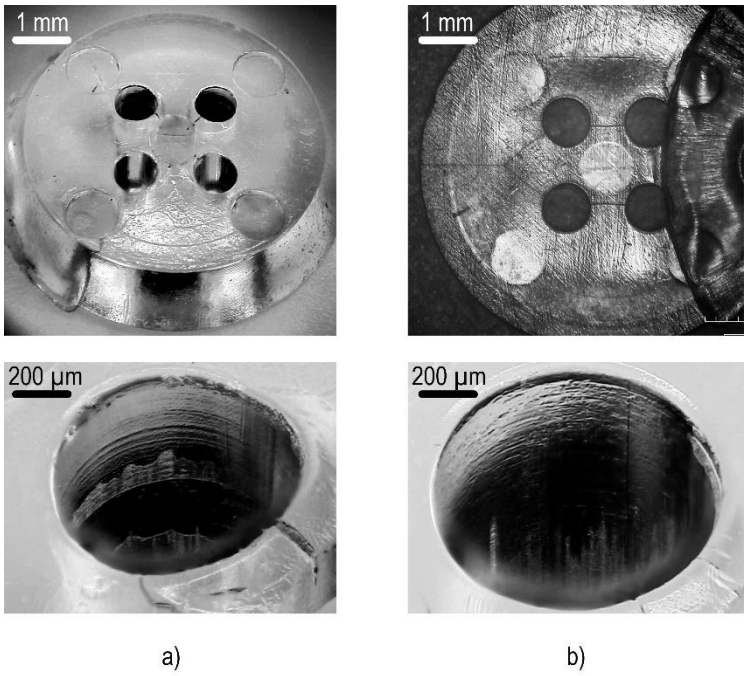

Figure 13: Produced molded parts with: a) mold Sample #1 and b) mold Sample #2)

4. Conclusions

Micromilling plays a key role on the process chains for producing polymer products trough µIM. In this work, footprint generation in micromilled deep cores, mimicking biochips applications, was controlled by selecting proper micromilling conditions. Two main approaches were adopted. The standard three-axis helicoidal approach caused strong tool dwelling, leading to unavoidable surface re-machining. Some combinations of micromilling machining parameters — above all the one with low feed per tooth, high spindle speed and low radial depth of cuts values — resulted in low surface roughness (down to Sa≃150 nm). The step-down approach resulted preferable to reduce the overall process variability and the tool contact time, producing more regular surface texture (with average Sa≃180 nm with more repeatable behavior among the cutting conditions). However, with this approach higher forces, higher average roughness and larger geometrical deviation on the pins (up to 10 µm) were showed. In this work, the surface footprint generation was modeled and phenomenologically explained trough the adoption of a mechanistic approach of micro cutting (to estimate the shape error considering the flexibility of tool and workpiece) and using statistical modeling (to estimate the texture generation).

Three representative molds were designed and manufactured by exploiting the above-mentioned models — they were machined with different µM strategies and parameters to produce three typical different footprints — and tested in µIM.

The molds' design with multiple deep cores in the cavity, was successful in enabling the conjunct performance analysis of the two micro manufacturing processes. It was in fact possible to isolate the impact of μM footprint on the demolding forces of μIM parts.

The acquired demolding forces showed a clear effect of the μM molds' quality. The demolding force peak was reported to increase by 250% by changing the finishing quality of the pins— i.e. by imposing different tribological conditions at the part-tool interface.

There are several areas for future work that can stem from this research. The first of which is modeling the mechanism behind the μM surface texture generation in complex 3-D features and using the developed models to optimize all the process chain. Additionally, further research will be devoted to study the μIM mold functionality by comparing μM performance with molds machined by other processes such as μEDM. The effect of different μIM parameters and the interaction effects between the micromilled molds quality and differ polymer materials will be also worth receiving further attention.

5. Acknowledgment

The present research work has been developed under the moral patronage of the Micro Manufacturing Engineering division of the Italian Association of Manufacturing Technology – AITeM. In addition, the authors want to acknowledge Engg. M.Camagni, and F.Cacciatore for their strong support in carrying out the experiments and other laboratory activities at the Politecnico di Milano and the Mahr® for supplying the WLI measuring system.

6. References

[1] Masato D, Sorgato M, Parenti P, Annoni M, Lucchetta G, Impact of deep cores surface topography generated by micro milling on the demolding force in micro injection molding, J Mater Process Tech, 246:211-223 · April 2017, DOI: 10.1016/j.jmatprotec.2017.03.028.

[2] Sasaki T, Koga N, Shirai K, Kobayashi Y, Toyoshima A, An experimental study on ejection forces of injection molding. J Prec Eng 2000; 24: 270-273.

[3] Yao D, Kim B, Scaling issues in miniaturization of injection molded parts. Journal of Manufacturing Science and Engineering 2004; 126(4): 733-739.

[4] Parenti P, Pagani L, Annoni M, Colosimo BM, Semeraro Q, On the geometrical accuracy of high aspect ratio micromilled pins. J Manuf Sci Eng ASME 2016; doi: 10.1115/1.4035035

[5] Masuzawa T, State of the art of micromachining. Annals of the CIRP 2000; 49: 473-488.

[6] Micro-Cutting: Fundamentals and Applications, First Edition. Edited by Kai Cheng and Dehong Huo, 2013 John Wiley & Sons, Ltd. Published 2013 by John Wiley & Sons, Ltd.

[7] Kim GM, Kim BH, Chu CN, Estimation of cutter deflection and form error in ball-end milling processes. Int J Mach Tool Manu 2003; 43(9): 917-924.

[8] Dornfeld D, Min D, Takeuchi S, Recent advances in mechanical micromachining. CIRP Annals - Manu Tech 2006; 5: 745-768.

[9] Fard MJB, Bordatchev EV, Experimental study of the effect of tool orientation in five-axis micro-milling of brass using ball-end mills. Int J Adv Manuf Technol 2013; 67:1079-1089

[10] Huo D, Cheng K, Wardle F, Design of a five-axis ultra-precision micro-milling machine- UltraMill. Part 1: holistic design approach, design considerations and specifications. Int J Adv Manuf Technol 2010; 47 (9): 867-877

[11] Denkena B, Böß V, Nespor D, Gilge P, Hohenstein S, Seume J, Prediction of the 3D Surface Topography after Ball End Milling and its Influence on Aerodynamics. 15th CIRP Conference on Modelling of Machining Operations.

[12] Liu X, Devor RE, Kapoor SG, Model-Based Analysis of the Surface Generation in Microendmilling- Part I: Model Development. J Manuf Sci Eng ASME 2007; 129(453)

[13] Kurczewski IP, Vehmeyer J, Simulation Model for micro-milling Operations and surface Generation. Advanced Materials Research 2011; 223: 849-858.

[14] Vehmeyer J, Hinduja S, Li L, A surface generation model for micro cutting processes with geometrically defined cutting edges. MATADOR 37th International Conference 2012, Manchester, 27(448): 582, 149-152.

[15] Liu H, Sun Y, Geng Y, Shan D, Experimental research of milling force and surface quality for tc4 titanium alloy of micro-milling. Int J Adv Manuf Technol 2015. 79 (1-4): 705-716.

[16] Elkaseer AMA, Dimov SS, Popov KB, Negm M, Minev R, Modeling the Material Microstructure Effects on the Surface Generation Process in Microendmilling of Dual-Phase Materials, J Manuf Sci Eng ASME 2012; 134: 44501-1

[17] Cai Y, Liu Z, Shi A, Song Q, Wan Y, Optimization of machining parameters for micro-machining nozzle based on characteristics of surface roughness, Int J Adv Manuf Technol 2015. 80 (5-8): 1403-1410.

[18] Annoni M, Rebaioli L, Semeraro Q, Thin wall geometrical quality improvement in micromilling. Int J Adv Manuf Technol 2015; 79:881-895.

[19] Leach RK, Characterisation of areal surface texture. Springer, 2013.

[20] Brinksmeier E, Riemer O, Twardy S, Tribological behavior of micro structured surfaces for micro forming tools, Int J Mach Tools Manufact 2010. 50 (4) 425-430.

[21] Guillemot N, Mawussi BK, Lartigue C, Billardon R, A first approach to characterize the surface integrity generated by ball-end finishing milling. Int J Adv Manuf Technol 2013; 64 (1-4): 269-279.

[22] Vakondios D, Kyratsis P, Yaldiz S, Antoniadis A, Influence of milling strategy on the surface roughness in ball end milling of the aluminum alloy al7075-t6. Measurement 2012; 45(6) 1480-1488.

[23] Kiswanto G, Zariatin DL, Ko TJ, The effect of spindle speed, feed-rate and machining time to the surface roughness and burr formation of aluminum alloy 1100 in micro-milling operation. Journal of Manufacturing Processes 2014; 16(4):435-450.

[24] Budak E, Altintas Y, Peripheral Milling conditions for improved dimensional accuracy. Int J Mach Tools Manufact 1994; 34(7): 907-918.

[25] Jin X, Altintas Y, Chatter Stability Model of Micro-Milling With Process Damping, J Manuf Sci Eng ASME 2013; 135: 031011.

[26] Jin X, Altintas Y, Prediction of micro-milling forces with finite element method. J Mater Process Tech 2012; 212: 542–552.

[27] Altintas Y, Jin X, Mechanics of micro-milling with round edge tools, CIRP Annals - Manu Tech 2011; 60: 77-80.

[28] Kops L, Vo DT, Determination of the Equivalent Diameter of an End Mill Based on its Compliance, CIRP Annals - Manu Tech 1990; 39: 93-96

[29] Kono D, Matsubara A, Ibaraki S, Ostubo H, Tsuboi M, Oshita I, Development and Evaluation of a High-Precision Machining Center with Friction-Less Drives. 11th International Conference on Precision Engineering (ICPE) 2006. August 16-18 Tokyo, Japan.

[30] ISO 4287: 1998. Geometrical product specification (GPS) - Surface texture: Profile method - Terms, definitions and surface texture parameters, International Organization for Standardization, Geneva, Switzerland.

[31] ISO 25178: Geometric Product Specifications (GPS) – Surface texture: areal. Part 1,2,3, International Organization for Standardization, Geneva, Switzerland.

[32] Masato D, Sorgato M, Lucchetta G, Analysis of the influence of part thickness on the replication of micro-structured surfaces by injection molding. Materials & Design 2016; 95: 219-224.

Appendix

Table 9: Complete μM conditions for Plan A and Plan B

Plan A)								
Test #	*Specimen*	*Run*	*Tool*	a_e	*N*	f_z	*cutting*
1	1	2	+	-	-	-	+
2	1	5	-	-	-	-	-
3	1	8	-	-	+	+	+
4	1	9	+	-	-	-	+
5	1	11	-	-	-	-	-
6	1	13	+	-	+	+	-
7	1	14	+	-	+	+	-
8	1	15	-	-	-	-	-
9	1	17	-	-	+	+	+
10	1	18	+	-	-	-	+
11	1	20	-	-	+	+	+
12	1	24	+	-	+	+	-
13	1	1	-	+	-	+	-
14	1	3	+	+	+	-	-
15	1	4	-	+	+	-	+
16	1	6	-	+	-	+	-
17	1	7	+	+	-	+	+
18	1	10	+	+	+	-	-
19	1	12	+	+	-	+	+
20	1	16	+	+	-	+	+
21	1	19	-	+	+	-	+
22	1	21	-	+	+	-	+
23	1	22	-	+	-	+	-
24	1	23	+	+	+	-	-

Plan A)								
Test #	*Specimen*	*Run*	*Tool*	a_e	*N*	f_z	*cutting*
25	2	1	-	-	-	+	-
26	2	4	-	-	-	+	-
27	2	6	+	-	+	-	-
28	2	10	+	-	-	+	+
29	2	13	+	-	+	-	-
30	2	14	-	-	+	-	+
31	2	15	+	-	-	+	+
32	2	16	+	-	+	-	-
33	2	17	-	-	-	+	-
34	2	19	-	-	+	-	+
35	2	22	-	-	+	-	+
36	2	24	+	-	-	+	+
37	2	2	-	+	-	-	-
38	2	3	+	+	+	+	-
39	2	5	+	+	+	+	-
40	2	7	-	+	-	-	-
41	2	8	-	+	-	-	-
42	2	9	-	+	+	+	+
43	2	11	-	+	+	+	+
44	2	12	-	+	+	+	+
45	2	18	+	+	-	-	+
46	2	20	+	+	-	-	+
47	2	21	+	+	+	+	-
48	2	23	+	+	-	-	+

Plan B)								
Test #	*Specimen*	*Run*	*Tool*	a_e	*N*	f_z	*Cutting*
49	3	20	-	-	+	+	+
50	3	5	+	+	+	+	+
51	3	13	-	+	+	-	+
52	3	1	-	+	-	+	+
53	3	21	+	+	-	-	+
54	3	12	-	-	+	+	+
55	3	2	+	-	+	-	+
56	3	19	+	+	+	+	+
57	3	11	+	-	-	+	+
58	3	23	-	+	+	-	+
59	3	4	-	-	-	-	+
60	3	10	-	+	-	+	+
61	3	17	+	-	-	+	+
62	3	18	+	+	-	-	+
63	3	6	-	-	-	-	+
64	3	22	-	+	-	+	+
65	3	3	+	-	+	-	+
66	3	9	+	-	-	+	+
67	3	8	+	+	+	+	+
68	3	16	+	-	+	-	+
69	3	24	-	-	+	+	+
70	3	7	-	-	-	-	+
71	3	14	+	+	-	-	+
72	3	15	-	+	+	-	+

Plan B)								
Test #	*Specimen*	*Run*	*Tool*	a_e	*N*	f_z	*Cutting*
73	4	7	+	-	-	-	+
74	4	12	+	-	-	-	+
75	4	24	+	-	+	+	+
76	4	2	-	-	+	-	+
77	4	19	-	-	+	-	+
78	4	8	+	+	-	+	+
79	4	9	-	+	-	-	+
80	4	18	+	+	-	+	+
81	4	13	-	-	-	+	+
82	4	20	-	+	-	-	+
83	4	3	-	+	+	+	+
84	4	4	-	+	-	-	+
85	4	15	+	-	-	-	+
86	4	6	+	+	+	-	+
87	4	23	-	-	+	-	+
88	4	14	-	+	+	+	+
89	4	21	+	+	-	+	+
90	4	1	+	-	+	+	+
91	4	16	+	+	+	-	+
92	4	5	-	-	-	+	+
93	4	22	-	-	-	+	+
94	4	10	-	+	+	+	+
95	4	11	+	-	+	+	+
96	4	17	+	+	+	-	+

Funding

This research did not receive any specific grant from funding agencies in the public, commercial or not-for-profit sectors.

Figure Captions

Table Captions